[3] Anderson, J. D., "Theory of Orbit Determination—Part II, Estimation Formulas," TR 32-498, Oct. 1963, Jet Propulsion Lab., Pasadena, Calif.
[4] Leighton, R. B., "The Surface of Mars," *Scientific American*, May 1970, Vol. 222 No. 5 pp. 26-41.
[5] Sharp, R. P. et al., "The Surface of Mars 4. South Polar Cap," *Journal of Geophysical Research*, Vol. 76, Jan. 1971, pp. 357-368.
[6] Danielson, G. E. and Montgomery, D. R., "Calibration of the Mariner Mars 1969 Television Cameras," *Journal of Geophysical Research*, Vol. 76, Jan. 1971, pp. 418-431.
[7] Davies, M. E. and Berg, R. A., "A Preliminary Control Net of Mars," *Journal of Geophysical Research*, Vol. 76, Jan. 1971, pp. 373-393.
[8] Campbell, J. K., "Mariner Mars 1969 Simulated Television Pictures—Final," Internal Document 605-237, June 1970, Jet Propulsion Lab., Pasadena, Calif.
[9] Dunne, J. A. et al., "Maximum Discriminability Versions of the Near-Encounter Mariner Pictures," *Journal of Geophysical Research*, Vol. 76, Jan. 1971, pp. 438-472.
[10] Duxbury, T. C., "A Spacecraft-Based Instrument for Outer-Planet Missions," AIAA Paper 69-902, Princeton, N.J., 1969.

AUGUST 1971 J. SPACECRAFT VOL. 8, NO. 8

Analytic Difficulties in Predicting Dynamic Effects of Separated Flow

LARS E. ERICSSON,* J. PETER REDING,† AND ROLF A. GUENTHER‡
Lockheed Missiles & Space Company, Sunnyvale, Calif.

The purpose of the paper is to demonstrate how a simple analytic theory that uses static experimental data as an input, can predict the observed large adverse effects of separated flow on the vehicle dynamics of heat-sink type re-entry bodies and elastic launch vehicles. The theory is based on quasi-steady-flow concepts in which the time history effects are lumped to one discrete past time event. The analytic difficulties consist largely of insufficient capability in predicting the composition of static loads in regions of separated flow, even when static experimental data are available. If more basic knowledge were available about nonsymmetric stationary separated flow, very substantial improvement in existing capability to predict dynamic effects of separated flow would result.

Nomenclature

A = axial force, kg, coefficient $C_A = A/(\rho U^2/2)S$
c = reference length, m (usually $c = d$)
d = body caliber, m
N = normal force, kg, coefficient $C_N = N/(\rho U^2/2)S$
L = longitudinal wake source distance, m
M = Mach number
M_P = pitching moment, kg-m, coefficient $C_m = M_P/(\rho U^2/2)Sc$
p = static pressure, kg/m^2
C_p = pressure coefficient $C_p = (p - p_\infty)/(\rho U^2/2)$
S = reference area, m^2, $S = \pi c^2/4$
t, Δt = time, and time lag, respectively, sec
U = freestream velocity, m/sec
$\bar{U}$ = mean convection velocity, m/sec
x,z = horizontal and vertical coordinates, respectively, m
ξ = dimensionless x coordinate, $\xi = x/c$
α = angle of attack, rad or deg
α_0 = trim angle of attack, rad or deg
β = equivalent spike deflection angle, rad or deg
Δ = difference
δ_F = flare rotation angle, rad or deg
ρ = air density, kg-sec^2/m^4
ω = pitching or bending frequency, rad/sec
$\bar{\omega}$ = reduced frequency, $\bar{\omega} = \omega c/U$
θ = body attitude, rad or deg

Subscripts

a = attached flow
C = cylinder
N = nose
QS = quasi-steady
s = separated flow
∞ = undisturbed flow

Superscripts

i = induced, e.g., $\Delta^i C_N$ = separation induced normal force
$'$ = induced by upstream communication, e.g., $C_{N_{\alpha'_s}}$
$\sim$ = generalized or effective value, e.g., $\tilde{\alpha}$

Differential symbols

$\dot{\theta}(t) = \partial\theta/\partial t$
$C_{N_\alpha} = \partial C_N/\partial\alpha$; $C_{m_\beta} = \partial C_m/\partial\beta$; $C_{N_\theta} = \partial C_N/\partial\theta$

Presented as Paper 70-762 at the AIAA 3rd Fluid and Plasma Dynamics Conference, Los Angeles, Calif., June 29–July 1, 1970; submitted August 6, 1970; revision received February 24, 1971.

* Senior Staff Engineer. Associate Fellow AIAA.
† Research Specialist. Member AIAA.
‡ Senior Aerodynamics Engineer.

Introduction

BOTH ascent and re-entry vehicles exhibit large regions of separated flow, especially in the transonic Mach number range. Heat-sink type re-entry bodies and the Saturn-Apollo launch vehicles exemplify cases where the aerodynamic loading is generated by "separated flow with embedded regions of attached flow." It is a well-known fact that simulation of boundary-layer separation and wake formation in a wind tunnel is very difficult for stationary flow, and is practically impossible in many cases for unsteady separated flow. As neither theory nor experiments alone can provide a solution, using both in combination is the only realistic approach.

Analysis

Quasi-steady forces are essentially static forces modified to account for slow perturbations from the static condition. The required slowness, $\bar{\omega}^2 \ll 1$, to make quasi-steady treatment applicable is fulfilled for rigid body oscillations of ascent and re-entry vehicles, and for elastic vehicle oscilla-

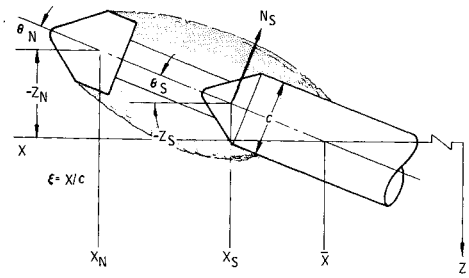

Fig. 1 Coordinate system for wake-induced loads.

tions in the three lowest bending modes (for the high velocities of practical interest here, e.g., the transonic speed region). The quasi-steady force coefficient in linearized form can be expressed as the product of the static force derivative obtained from static experimental data, and an effective angle of attack suitably modified to account for slow perturbations from the static value. That is

$$C_{N_{QS}} = C_{N_{\text{static}}} + \tilde{C}_N = C_N(\alpha_0) + C_{N_\alpha}\tilde{\alpha} \tag{1}$$

In classical quasi-steady theory $\alpha_0 + \tilde{\alpha}$ is the local instantaneous crossflow angle

$$\alpha_0 + \tilde{\alpha} = \alpha_0 + \theta + (\dot{z}/U) \tag{2}$$

This formulation is valid for aerodynamic forces that are dependent only upon local conditions. This is only a small portion of the aerodynamic load on a body element submerged in separated flow. The main portion of the load is dependent upon conditions upstream at the separation source (with the additional requirement that so-called upstream communication effects are negligible; see later discussion of near wake effects). One can express this separation-induced loading in the following form:

$$\Delta^i C_{N_{QS}} = \Delta^i C_N(\alpha_0) + \Delta^i C_{N\alpha}\tilde{\alpha} \tag{3}$$

The separation-induced load at time t, $\tilde{\Delta}^i C_N(t)$, is dependent upon the separation-inducing generalized angle of attack at an earlier time, $t - \Delta t$. That is

$$\tilde{\Delta}^i C_N(t) = \Delta^i C_{N\alpha}\tilde{\alpha}(t - \Delta t) \tag{4}$$

In the situation depicted in Fig. 1, let us assume that the body is rigid, describing oscillations around $\bar{x}$. The elastic body describing bending oscillations can be treated in an analogous manner.[1,2]

The quasi-steady force N_s of the body component submerged in separated flow can be expressed as follows in coefficient form:

$$\begin{aligned} C_{N_s} &= \tilde{C}_N(t) + \tilde{\Delta}^i C_N(t) \\ C_N(t) &= C_{N\alpha_s}\tilde{\alpha}_s(t) \\ \tilde{\Delta}^i C_N(t) &= \Delta^i C_{N\alpha}\tilde{\alpha}_N(t - \Delta t) + \Delta^i C_{N\beta}\beta(t - \Delta t) \end{aligned} \tag{5}$$

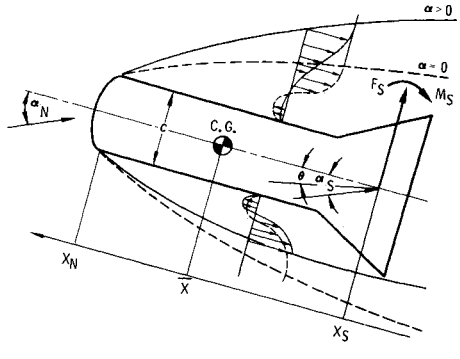

Fig. 2 Coordinate system for nose-induced separation.

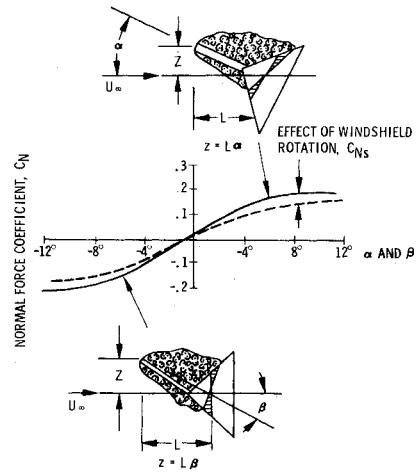

Fig. 3 Comparison of angle of attack and spike deflection effects.

where

$$\begin{aligned} \alpha_s(t) &= \theta(t) - (x_s - \bar{x})\theta(t)/U \\ \alpha_N(t - \Delta t) &= \theta(t - \Delta t) - (x_N - \bar{x})\theta(t - \Delta t)/U \\ \beta(t - \Delta t) &= [(x_N - \bar{x})/(x_N - x_s)]\theta(t - \Delta t) - \\ &\qquad [(x_s - \bar{x})/(x_N - x_s)]\theta(t) \end{aligned}$$

For slow oscillations of modest amplitudes

$$\theta(t - \Delta t) \approx \theta(t) - \Delta t\dot{\theta}(t),\ \dot{\theta}(t - \Delta t) \approx \dot{\theta}(t) \tag{6}$$

Thus, $\tilde{\alpha}_s(t)$, $\tilde{\alpha}_N(t - \Delta)$ and $\beta(t - \Delta t)$ can be written in the following form:

$$\tilde{\alpha}_s(t) = \theta(t - \tilde{\Delta}t_s),\quad \tilde{\alpha}_N(t - \Delta t) = \theta(t - \Delta t - \tilde{\Delta}t_N) \tag{7}$$

$$\beta(t - \Delta t) = [(\xi_N - \bar{\xi})/(\xi_N - \xi_s)\theta(t - \Delta t) - [(\xi_s - \bar{\xi})/(\xi_N - \xi_s)]\,\theta(t)$$

where

$$\tilde{\Delta}t_s = (\xi_s - \bar{\xi})c/U,\ \tilde{\Delta}t_N = (\xi_N - \bar{\xi})c/U$$

$$\Delta t = (U/\bar{U})(\xi_N - \xi_s)c/U$$

Δt is the true time lag determined by the mean velocity, $\bar{U} \leq U$, with which the effects of crossflow changes at x_N are convected through the separated flow down to the submerged

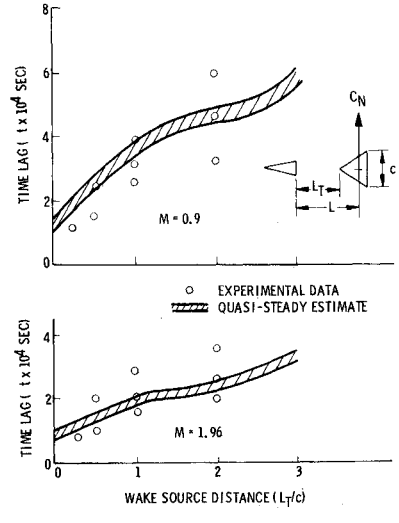

Fig. 4 Comparison between estimated and measured time lags as a function of downstream distance from a conical wake source.

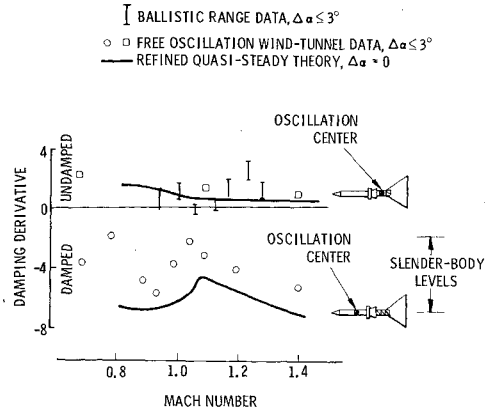

Fig. 5 Comparison between quasi-steady predictions and experimental data for the Apollo escape system configuration.

body element at x_s. The quantities $\tilde{\Delta}t_s$ and $\tilde{\Delta}t_N$ are generalized time lags corresponding to the effect of mechanical or structural phasing. For the $\bar{x}$ value shown in Fig. 1, both $\tilde{\Delta}t_s$ and $\tilde{\Delta}t_N$ are positive, representing lag effects. That is, the negative crossflow angles, $-(x_s - \bar{x})/U$ and $-(x_N - \bar{x})/U$, induced by the pitch velocity, oppose the body attitude, θ, and the resultant generalized crossflow angles lag the body attitude. When the oscillation center $\bar{x}$ is forward of x_s or x_N, the pitch-velocity-induced crossflow amplifies the body attitude causing the resultant generalized crossflow angle to lead the body attitude ($\tilde{\Delta}t_s$ and $\tilde{\Delta}t_N$ negative).

The wake sources can have very different wake-directing effects.[2] A disk or sharp-edged blunt wake source leaves a wake aligned with the freestream, i.e., the effect of α_N is zero, $\Delta^i C_{N_\alpha} = 0$, and the translatory derivative $\Delta^i C_{N_\beta}$ is the only wake-induced effect. A blunt ogive-cylinder wake source produces separated flow ahead of its base thus producing an initial upward movement of the wake, adding $\tilde{\Delta}^i C_{N_\alpha} > 0$ to the pure translatory derivative $\Delta^i C_{N_\beta}$. A slender wake source directs the wake initially along its centerline and thus downward from the freestream direction, producing a negative derivative, $\Delta^i C_{N_\alpha} < 0$.

If the cylindrical wake source support in Fig. 1 is made increasingly larger in diameter, it starts directing the wake more and more experiencing aerodynamic forces in the process. Finally, when the support and nose diameters are the same, the translatory wake derivative disappears $\Delta^i C_{N_\beta}$

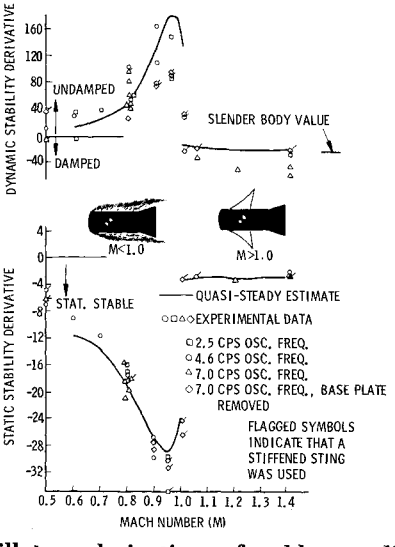

Fig. 6 Oscillatory derivatives of a blunt cylinder-flare body for 1.0° amplitude oscillations around $\alpha = 0$.

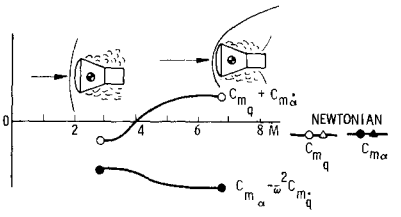

Fig. 7 Oscillatory derivatives of a blunt re-entry capsule.

$= 0$. That is, the center of the wake no longer moves. The wake boundaries move, however, and the flow geometry sketched in Fig. 2 is realized.

The wake directing effect of α_N still exists. However, the directing effect is no longer accomplished by a translatory displacement, as was the case for the free wake, but is produced instead through changes in the wake shear flow profiles, compressing and steepening of windward side shear profile, and opposite effects on the leeward side. That is, the nose angle of attack α_N induces a flare force that mathematically abides by Eq. (5) with $\Delta^i C_{N_\beta} = 0$.

Prediction of Dynamic Data

The tip of a thin flow separation spike is a good example of a nondirecting wake source. Results obtained for a conical heat shield[3] shows that it is the wake translation across the submerged body that produces the main force change (Fig. 3). It is obvious that it takes a finite time before the effect of the translation of the wake generator has been convected downstream to the submerged body.

Using forebody axial force deficit on the submerged body to define an average convection velocity in an incompressible wake

$$\bar{U} = U(C_{A_F})_s^{1/2}/(C_{A_F})_a^{1/2}$$

gives the time lag shown in Fig. 4. The agreement with experiments[4] is rather good. Using this time lag based on the average wake velocity ($\bar{U}$) in a quasi-steady analysis together with static experimental data[4] gives the prediction of the damping derivative of the Saturn-Apollo escape system shown in Fig. 5. The agreement with dynamic measurements[5,6] is good. It is especially noteworthy that the measured undamping for the nondirecting wake source, the disk-on escape rocket, is predicted.

The blunt, flared re-entry body experiences similar large flow separation effects at transonic speeds. Using downstream convective time lags and static experimental data in a quasi-steady analysis[2,7] gives good prediction of the dynamic instability measured at subsonic speeds (Fig. 6). The op-

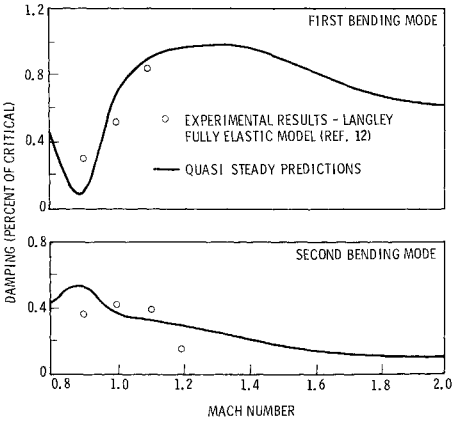

Fig. 8 Correlation of refined aerodynamic damping predictions and experimental data for an elastic Saturn I-Apollo vehicle with flow-separation disk.

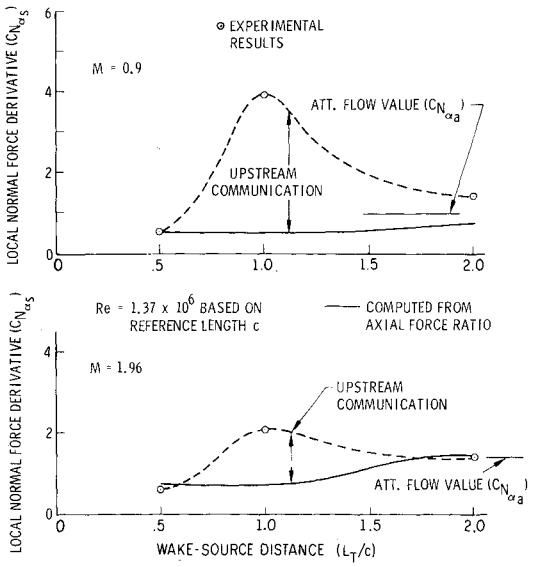

a) SUBMERGED BODY LOADS

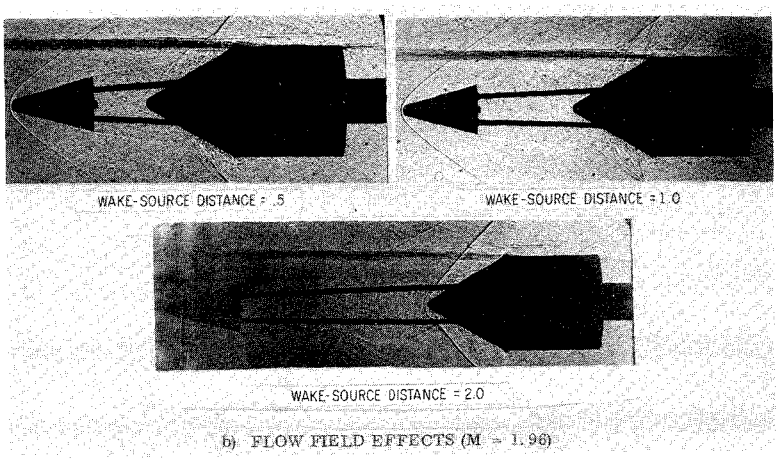

b) FLOW FIELD EFFECTS (M = 1.96)

Fig. 9 Aerodynamic characteristics of bodies in wakes.

position between the effects of flow separation on static and dynamic stability is caused by the time lag associated with finite convection velocities. The reattaching (at least partially) flow on the flare of the re-entry body at high subsonic speeds and the reattaching flow on the aft body of re-entry capsules at hypersonic or high supersonic speeds show great similarities, and the same statically stabilizing, dynamically destabilizing effects are observed[8–11] (Fig. 7).

Applying the same quasi-steady analysis technique to the elastic Saturn-Apollo launch vehicle with its complicated separated flowfield predicts dynamic measurements[12] quite well (Fig. 8). In fact, the accuracy has been judged to be satisfactory for prediction of low frequency launch vehicle buffet.[13]

Analytic Difficulties

The purpose of the preceding discussion has been to convince the reader that it is not impossible to predict dynamic effects of separated flow, and that it is, therefore, not meaningless to discuss the analytic difficulties encountered in this quasi-steady analysis. Only downstream convection and associated time lag was considered in the described analysis. It was, therefore, somewhat of a shock to measure the characteristics shown in Fig. 9, which demonstrate with all desired clarity that upstream communication from the submerged body to the wake generator exists, and that the resulting changes in the wake generates large loads on the submerged body. The neglect of this upstream communication did not upset the predictions of the Saturn-Apollo vehicle dynamics because the submerged command module is "inside" the "wake neck" for the short tower used to mount the escape-rocket on the command module. However, when the submerged body is in or near the "neck" of the free wake, large effects can be expected, resulting in decelerator instability[14] and dynamic sting interference problems.[8,15]

The flowfield existing with a body in the wake needs to be investigated further, both theoretically and experimentally. The unperturbed flowfield has received most of the attention so far. More research is needed determining the effects of crossflow and body deflections on static characteristics. With a better understanding of the steady-state conditions, improved prediction of the unsteady characteristics could be accomplished using the quasi-steady approach described here. It should be emphasized that the quasi-steady technique is valid only for slow oscillations, such as rigid body oscillations or elastic oscillations in the lower bending modes.

Vortices in Separated Flow

When turbulent flow separation is caused by a shock generated by a flare or interstage frustum, the perturbations from axisymmetry can cause very dramatic flow changes (Fig. 10a). The flow deviates very substantially from the classic picture.[16,17] At $\alpha = 0$ two pairs of circumferentially distributed vortices are observed (Fig. 10a). The vortex pattern is extremely sensitive to angle of attack. At $\alpha = 4°$ a single pair of leeward side vortices exist (Fig. 10b). These strong leeward side vortices appear to be fed from the windward side reattachment zone and shed into the wake over the

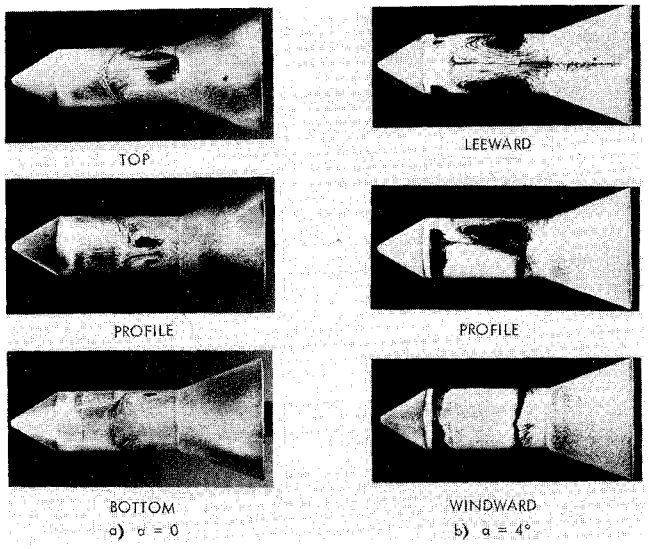

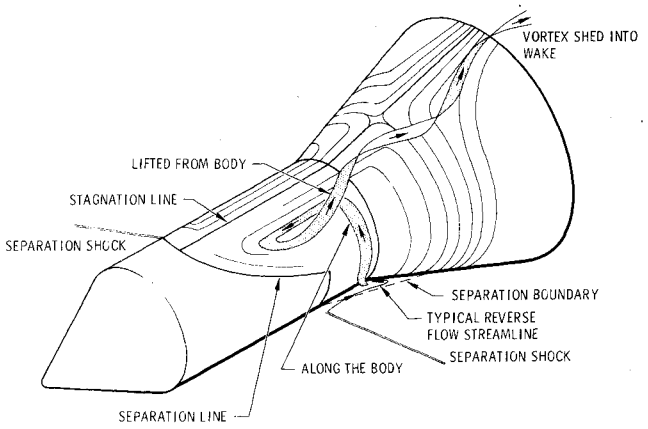

Fig. 10 China clay flow patterns, $\xi_C = 2.0$, $M = 1.2$.

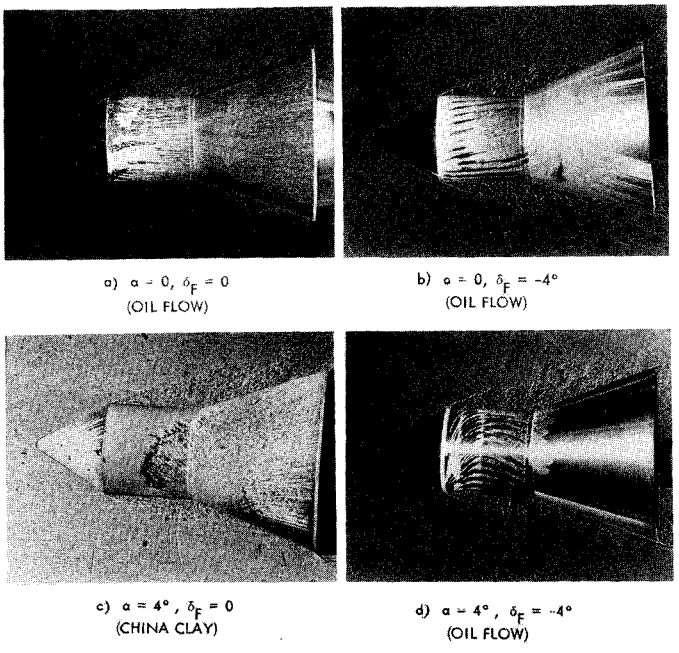

Fig. 11 Flow patterns for nose-induced separation ξ_C = 1.0, M = 0.9.

leeward side flare shoulder (see flow sketch inset in Fig. 10). The orientation of the twin vortex pair at $\alpha = 0$ was random.[16] Coe has recently obtained similar results for flared bodies,[18] and Ginoux,[19,20] Roshko,[21] and Uebelhack[21,22] have shown similar vortex structures in the separated flow regions generated by forward and backward facing steps.

Similar interesting results were obtained for nose-induced separation at $M = 0.9$.[17] Figure 11 shows that the flow at

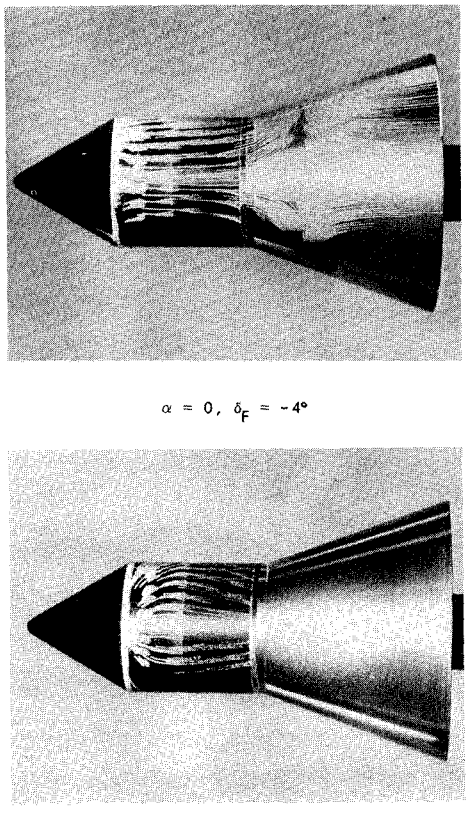

Fig. 12 Bottom or windward side flow patterns, ξ_C = 1.0, M = 0.9.

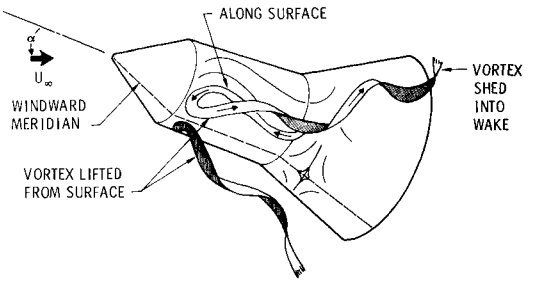

Fig. 13 Flow model for nose-induced separation.

$\alpha = 0$ over a one-caliber cylinder is not strictly axisymmetric, if one judges from the streamline curvature near the cone shoulder and in the reattachment zone on the flare (Fig. 11a). Pitching the flare causes an inclination of the streamlines in the recirculation region opposite to the flare attitude (Fig. 11b). Thus, the "flipping" of the wake postulated earlier[14,17] (Fig. 9) is verified, and a strong upstream communication effect is indicated. Pitching the entire cone-cylinder flare configuration gives a highly curved flow in the recirculation region over the cylinder (Fig. 11c). This flow is reduced by an upward deflection of the flare (Fig. 11d).§ For both the angle-of-attack and the flare deflection cases, there is a tendency for the streamlines to converge at the bottom of the cylinder at the cone-cylinder shoulder where the suction peak occurs.[1,2] Typical flow visualization photographs of the bottom of the model give no distinct indication of shed vorticity in the plane of the surface (Fig. 12). However, the converging surface streamlines must be vented in some manner (i.e., they indicate a sink). The flow model shown in Fig. 13 is suggested. The separated region is vented through a pair of counter rotating vortices. For longer cylinders at $M = 0.9$, the vortices are not confined to the cone-cylinder shoulder, and vorticity can again be observed on the cylinder aft of the shoulder (Fig. 14).

When the cylinder length is increased further to $\xi_C = 4.5$, the flowfield at $M = 0.9$ changes considerably. The flow over the cone shoulder is attached, but a local separation is induced by the terminal normal shock (Fig. 15a). This is similar to the shock-induced vortex patterns observed by Chevalier.¶[24] At angle of attack, the leeward-side boundary

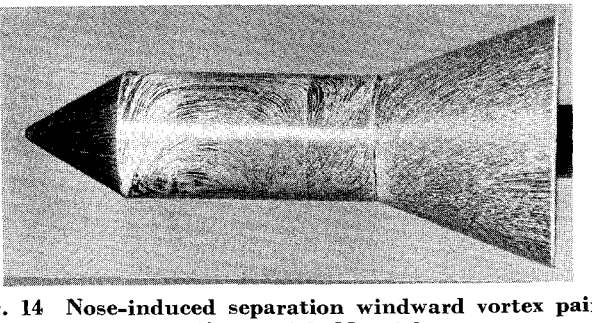

Fig. 14 Nose-induced separation windward vortex pair, $\alpha = 4°$, $\xi_C = 2.0$, $M = 0.9$.

§ Two flow visualization techniques are involved here. Figures 11a, 11b, and 11d involve an oil dot technique,[23] whereas Fig. 11c utilizes a modified china-clay technique. Here the model was sprayed with a mixture of china-clay and oil-of-wintergreen and the resulting flow patterns were photographed. In the former case, the streaking of a series of small oil dots illustrates the flowfield.

¶ It is possible that that oil dot size (the oil dot technique was used) may affect the scale of the vorticity; however, it does not affect the basic phenomenon (i.e., the vortices would still be there without oil).

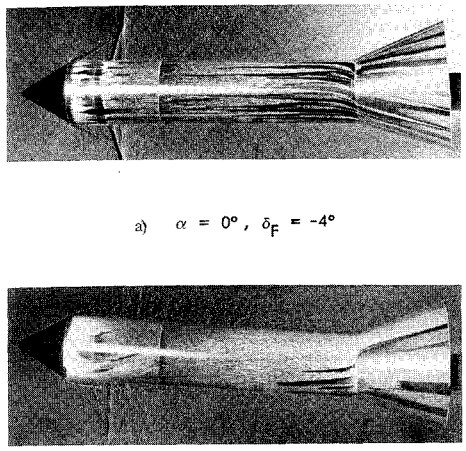

a) $\alpha = 0°$, $\delta_F = -4°$

b) $\alpha = 4°$, $\delta_F = -4°$

Fig. 15 Effect of angle of attack on retarded separation flow patterns, $\xi_C = 4.5$, $M = 0.9$.

layer is weakened and the separation jumps to the shoulder, producing the usual nose-induced separated flowfield with its large scale vorticity (Fig. 15b). The influence of the flare is restricted to the region just upstream of the flare and does not interact with the nose-induced separated flow region. Thus, upstream communication effects should not be significant at subsonic speeds for long cylinder-flare bodies such as this.

As one would expect, the effect of upstream communication does not vanish for long cylinder-flare bodies when the separation is induced by the flare shock (Fig. 16). The most striking feature of the effect of flare deflection (upwards) on shock-induced separation at $\alpha = 0°$ is illustrated by the correlation between the shadowgraph and the china-clay flow photograph (superimposed in Fig. 16). The flow near the lateral meridian is turned downward by the slightly skewed flare shock, but

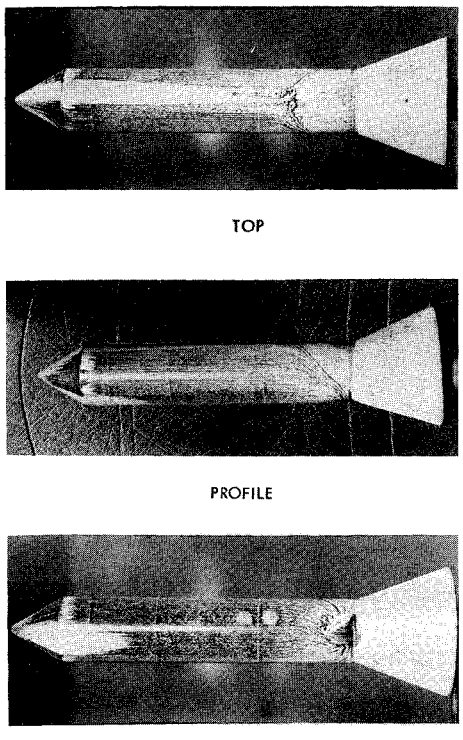

TOP

PROFILE

BOTTOM

Fig. 16 Shock-induced separation upstream communication flow patterns, $\xi_C = 4.5$, $M = 1.2$, $\alpha = 0°$, $\delta_F = -4°$.

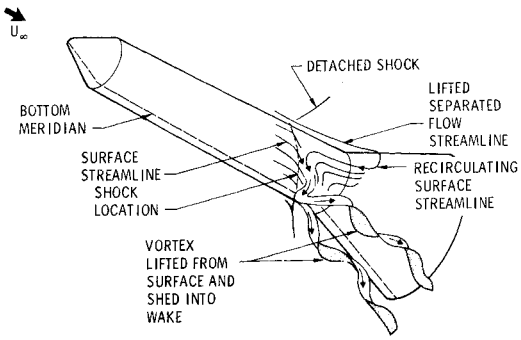

Fig. 17 Shock-induced separation upstream communication flow model, $\alpha = 0$, $\delta_F \neq 0$.

does not separate.** The flow along the bottom of the cylinder penetrates the shock without separating until just forward of the flare. At the leeward meridian, the flow separates in a nearly two-dimensional manner. This recirculating flow along the top surface is pulled down by the unseparated flow along the lateral portions of the cylinder and converges on the bottom cylinder-flare juncture. The flow model shown in Fig. 17 is, therefore, suggested. It essentially describes the flowfield seen in the photographs, but proposes a pair of shed vortices (similar to the model for nose-induced separation on a short cylinder) that vents the flow converging at the bottom cylinder-flare juncture.††

Forebody crossflow dominates the shock-induced separation to an even greater extent than it does nose-induced separation (Fig. 18). Crossflow thickens and weakens the leeward-side boundary layer by sweeping low-energy fluid to the leeward side, and a corresponding strengthening of the windward boundary-layer results. Thus, separation is promoted on the leeward side, resulting in a forward movement and a weakening of the leeward-side detached flare shock. The flow photographs (Fig. 18) indicate a large leeward-side separation while on the windward side the flow is attached aft of the shock. (The vorticity may play a part in energizing and reattaching the windward boundary layer immediately aft of the shock. The windward-side flow is then swept to the leeward side (by the transverse pressure gradient resulting from the unequal windward and leeward-side shock strength), after stagnating at the cylinder-flare juncture. This flow and the recirculating separated flow near the leeward meridian combine to feed large lateral vortices generating essentially the flow pattern sketched in Fig. 10.

Close examination of Fig. 18 reveals that the flare, via upstream communication, has a small effect on the flow patterns. That is, the existence of some minor upstream communication effect is indicated.

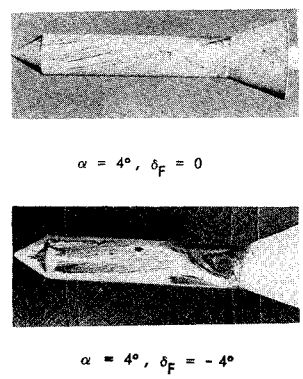

$\alpha = 4°$, $\delta_F = 0$

$\alpha = 4°$, $\delta_F = -4°$

Fig. 18 Effect of upstream communication on shock-induced separation flow patterns at $\alpha = 4°$, $M = 1.2$, $\xi_C = 4.5$.

** The shock location may be traced around the body by connecting the locus of points where the streamlines begin to turn.

†† The existence of these vortices is indicated by the thick turbulent shear layer visible on the shadowgraph which correlates with the proposed origin of the vorticity.

Conclusions

The presented results show that 1) dynamic effects of separated flow can be predicted, and 2) basic research of cross-flow effects on stationary separated flow is needed to corroborate and extend existing knowledge of unsteady separated flow. In particular, the effects of experimentally observed large-scale vortices in "axisymmetric" or "two-dimensional" separated flow need to be understood better. Since the dynamic effects of separated flow usually are much larger than the static effects, and in addition, often adverse, it is important to improve our predicting capability.

References

[1] Ericsson, L. E. and Reding, J. P., "Analysis of Flow Separation Effects on the Dynamics of a Large Space Booster," *Journal of Spacecraft and Rockets*, Vol. 2, No. 4, July-Aug. 1965, pp. 481–490.

[2] Ericsson, L. E. and Reding, J. P., "Dynamics of Separated Flow over Blunt Bodies," Rept. 2-80-65-1, Contract NAS 8-5338, Dec. 1965, Lockheed Missiles & Space Co., Sunnyvale, Calif.

[3] Harman, R. W. and Boatright, W. B., "Investigation of the Aerodynamic Characteristics of a Re-Entry Capsule with Various Nose Shapes at a Mach Number of 2.91, Including Studies of Nose Spikes as a Means of Control," TMX-426, Jan. 1961, NASA.

[4] Ericsson, L. E. and Reding, J. P., "Aeroelastic Characteristics of Saturn 1B and Saturn V Launch Vehicles," Technical Summary Report, M-37-67-5, Contract NAS 8-11238, Dec. 1967, Lockheed Missiles & Space Co., Sunnyvale, Calif.

[5] Lowndes, R. I. and Shadow, T. O., "Transonic Static and Dynamic Stability Characteristics of Several Saturn 1B and V Upper Stage Configurations," TR-66-125, June 1966, Arnold Engineering Development Center, Tullahoma, Tenn.

[6] Ballistic Range Data, Ballistic Research Labs, Aberdeen, Md., unpublished.

[7] Ericsson, L. E., "Separated Flow Effects on the Dynamic Stability of Blunt-Nosed Cylinder-Flare Bodies," LMSC-667991, Contract NAS 8-5338, Dec. 1965, Lockheed Missiles & Space Co., Sunnyvale, Calif.

[8] Ericsson, L. E. and Reding, J. P., "Aerodynamic Effects of Bulbous Bases," CR-1339, Aug. 1969, NASA.

[9] Ericsson, L. E., and Reding, J. P., "Re-Entry Capsule Dynamics;" also *Journal of Spacecraft and Rockets*, Vol. 8, No. 6, June 1971, pp. 575–586.

[10] Fletcher, H. S., "The Damping in Pitch and Static Stability of Supersonic Impact Nose Cones, and Manned Re-Entry Capsules at a Mach Number of 6.83," TMX 349, Jan. 1961, NASA.

[11] Fletcher, J. S., "Damping in Pitch and Static Stability of Blunt Cone-Cylinder Flare Models and Manned Re-Entry Capsule Models for Various Angles of Attack at a Mach Number of 2.91," TMX-539, July 1961, NASA.

[12] Hanson, P. W. and Dogget, R. V., Jr., "Aerodynamic Damping and Buffet Response of an Aeroelastic Model of the Saturn I Block II Launch Vehicle," TND-2713, March 1965, NASA.

[13] Rainey, A. G., "Progress on the Launch Vehicle Buffeting Problem," *Journal of Spacecraft and Rockets*, Vol. 2, No. 3, May-June 1965, pp. 289–299.

[14] Reding, J. P. and Ericsson, L. E., "Loads on Bodies in Wakes," *Journal of Spacecraft and Rockets*, Vol. 4, No. 4, April 1967, pp. 511–518.

[15] Reding, J. P. and Ericsson, L. E., "Dynamic Support Interference—Fact or Fiction?" AIAA Paper 71-277, Albuquerque, N. Mex., 1971.

[16] Reding, J. P., Guenther, R. A., Ericsson, L. E., and Leff, A. D., "Nonexistence of Axisymmetric Separated Flow," *AIAA Journal*, Vol. 7, No. 7, July 1969, pp. 1374–1375.

[17] Ericsson, L. E., Reding, J. P., and Guenther, R. A., "Effects of Shock-Induced Separation," Technical Summary Report L-87-69-1, Contract NAS 8-20354, Dec. 1965, Lockheed Missiles & Space Co., Sunnyvale, Calif.

[18] Coe, C. F., private communication, 1968, NASA Ames Research Center.

[19] Ginoux, J. J., "Experimental Evidence of Three-Dimensional Perturbations in the Reattachment of a Two-Dimensional Laminar Boundary Layer at M = 2.05," TN 1, Nov. 1958, von Kármán Institute for Fluid Dynamics, Rhode-Saint-Genese, Belgium.

[20] Ginoux, J. J., "On Some Properties of Reattaching Laminar and Transitional High Speed Flows," TN 53, Sept. 1969, von Kármán Institute for Fluid Dynamics, Rhode-Saint-Genese, Belgium.

[21] Roshko, A. and Thomke, G. J., "Observations of Turbulent Reattachment Behind an Axisymmetric Down-Stream Facing Step in Supersonic Flow," *AIAA Journal*, Vol. 3, No. 6, June 1966, pp. 975–980.

[22] Uebelhack, H. T., "Turbulent Flow Separation Ahead of Forward Facing Steps in Supersonic Two-Dimensional and Axisymmetric Flows," TN 54, July 1969, von Kármán Institute for Fluid Dynamics, Rhode-Saint-Genese, Belgium.

[23] Meyer, R. F., "A Note on a Technique of Surface Flow Visualization," NRC LR-457, July 1966, National Aeronautical Establishment, Ottawa, Canada.

[24] Chevalier, H. L., private communication, NASA Ames Research Center (presently at Texas A&M).